Synthesis of Surface Grown Pt Nanoparticles on Edge-enriched MoS_2 Porous Thin Films for Enhancing Electrochemical Performance

Sha Li[1], Ja Kyung Lee[1], Si Zhou[1], Mauro Pasta[1], Jamie H. Warner[1*]*

[1]Department of Materials, University of Oxford, 16 Parks Road, OX1 3PH, UK

Email: jamie.warner@materials.ox.ac.uk; mauro.pasta@materials.ox.ac.uk;

Supporting Information

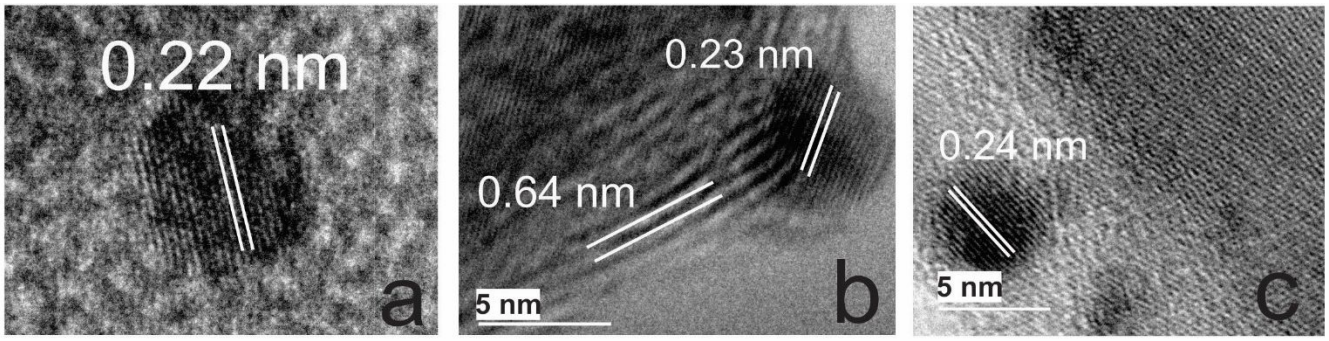

Figure S1. High resolution TEM image of one specific Pt nanoparticle deposited on MoS_2 for precursor loading of (a) 11 wt%, (b) 1.1 wt% and (c) 0.11 wt%. The white lines measure interlayer spacing $d_{(001)}$ in MoS_2 of 0.64nm and $d_{(111)}$ in Pt crystal of 0.23nm, respectively.

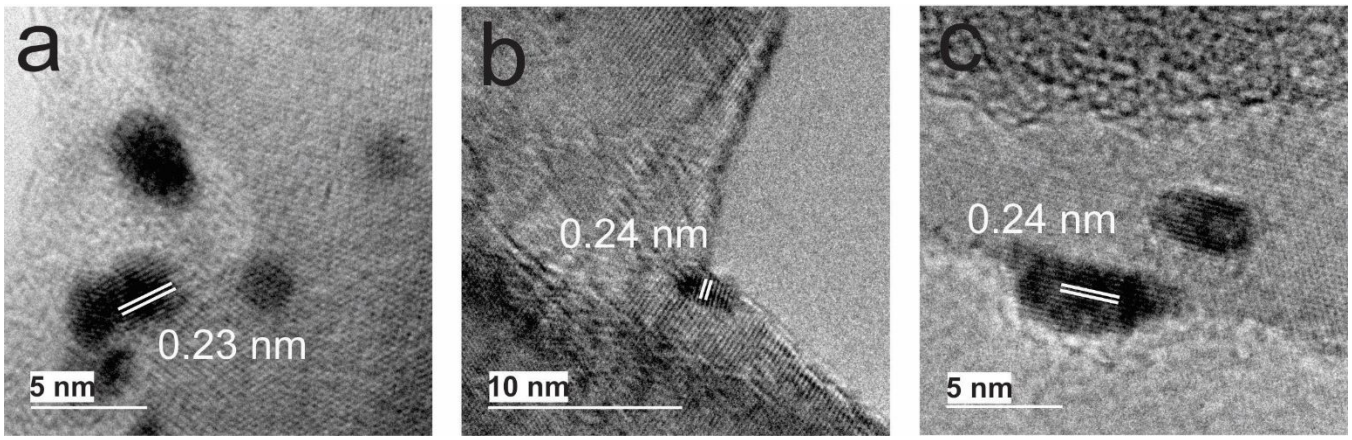

Figure S2. High resolution TEM images of Pt nanoparticles deposited on MoS_2 for thermal annealing temperature of (a) 400 °C, (b) 500 °C and (c) 600 °C. The white lines measure interlayer spacing $d_{(111)}$ in Pt crystal.

Table S1. EDX quantitative elemental analysis based composition determination of Pt-MoS_2 catalyst synthesized with 10 mM $H_2PtCl_6 \cdot 6H_2O$:ethanol, annealed at 400 °C for 40 mins.

Spot	Atomic % of element Mo	Atomic % of element Pt
1	29.56	3.42
2	29.56	3.32
3	31.38	3.90
4	30.85	3.57
5	30.70	3.29
6	31.56	4.41
7	31.97	2.88
8	31.22	3.59
Average	30.85	3.5475

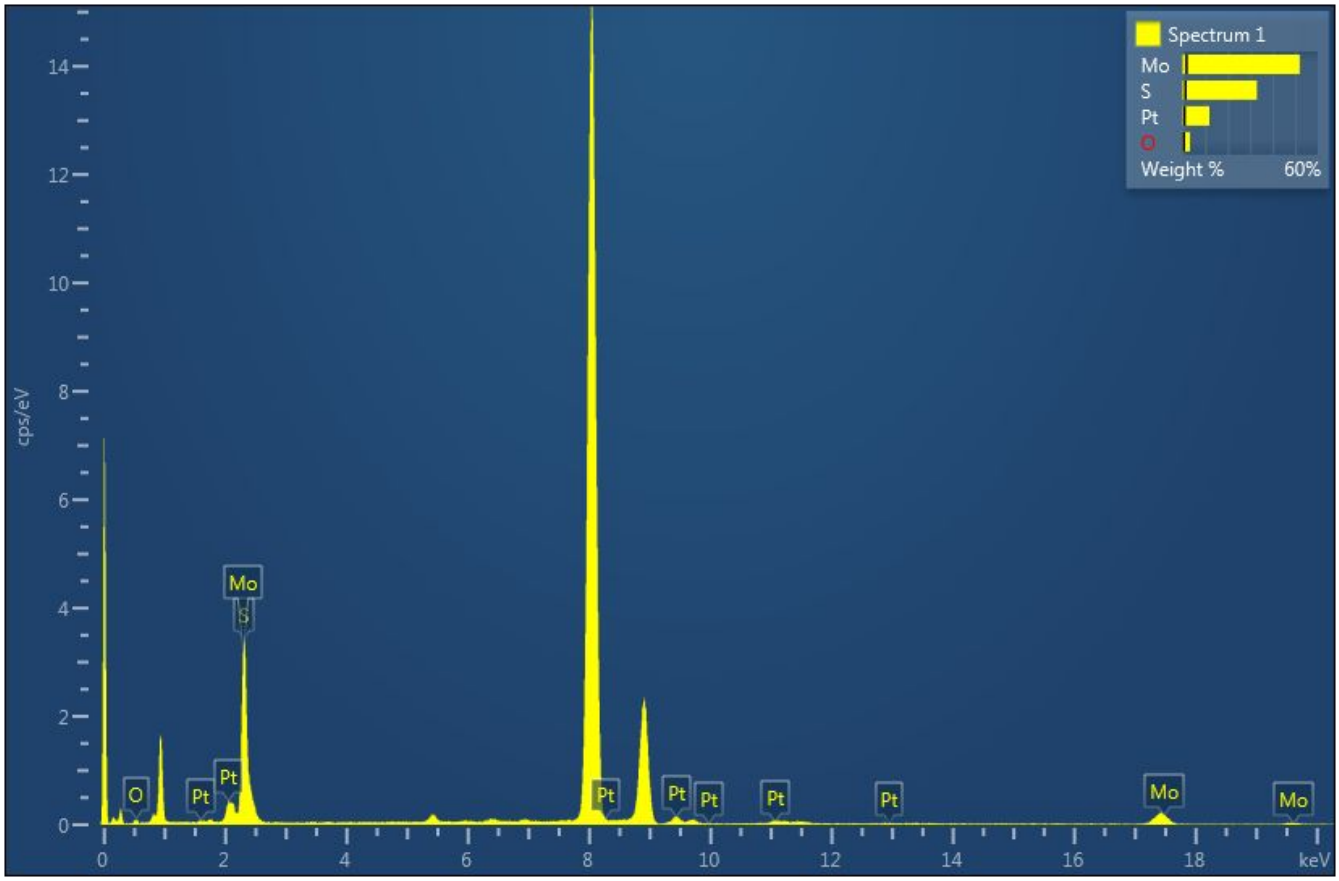

Figure S3. EDX spectrum of Pt-MoS_2 catalyst synthesized with 10 mM $H_2PtCl_6 \cdot 6H_2O$:ethanol, annealed at 400 °C for 40 mins.

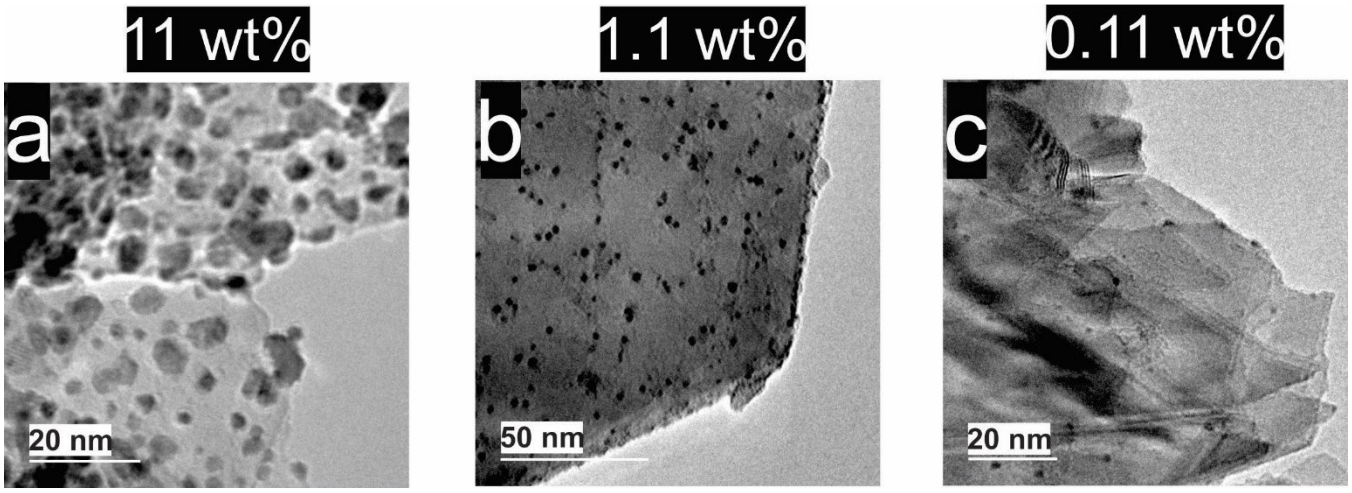

Figure S4. TEM images of Pt-MoS_2 at Pt wt% of 11 wt%, 1.1 wt% and 0.11 wt% at TA temperature of 500 °C for 40 mins.

Table S2. Summary of Pt-MoS_2 catalytic activity (onset potential, Tafel slope and exchange current density) for electrochemical water splitting process.

Catalysts	Onset Potential (mV vs RHE)	Tafel Slope (mV/dec)	Exchange Current Density (μA/cm^{-2})
10mM Pt – 400C H_2 40min	9	44	373
1mM Pt – 400C H_2 40min	65	68	27
0.5mM Pt – 400C H_2 40min	68	74	15
0.1mM Pt – 400C H_2 40min	359	82	1.9
0.1mM Pt – 500C H_2 40min	130	65	0.7
1mM Pt – 500C H_2 40min	281	53	0.58
10mM Pt – 500C H_2 40min	122	31	1.54
0.1mM Pt – 600C H_2 40min	210	139	3.5
0.1mM Pt – 500C H_2 20min	103	84	1.9
0.1mM Pt – 500C H_2 80min	128	80	0.5

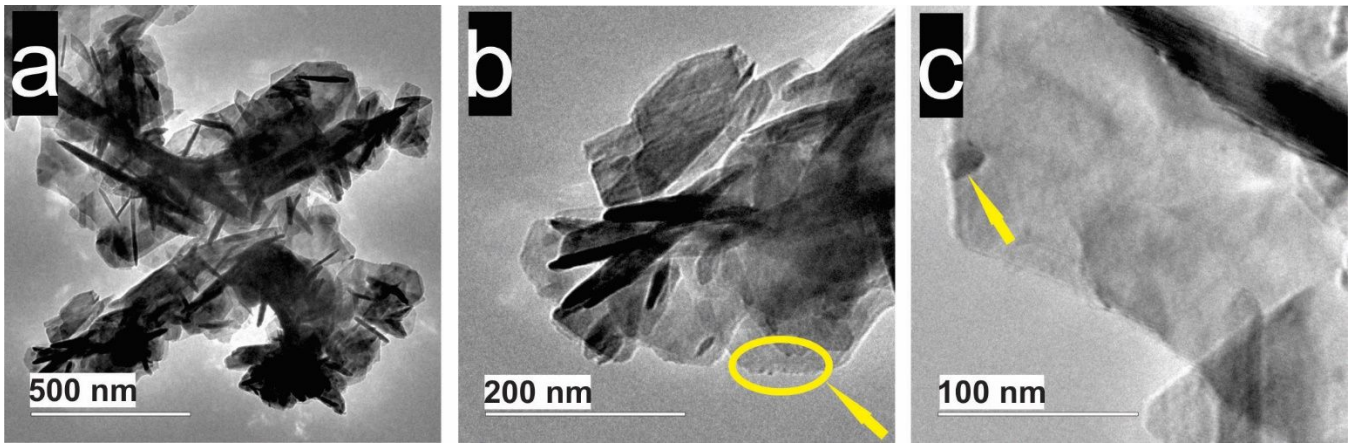

Figure S5. TEM image of Pt precursor coated MoS_2 thermal annealed in pure Ar gas (0.11 wt% Pt, 500 °C, 40mins). A small amount of Pt nanoparticles are formed in the circled area and indicated by the arrow.

Table S3. Summary of literature catalytic parameters towards HER of Pt supported catalysts. (Pt alloy systems not included)

Catalyst	**Media**	**Pt loading (μg/cm²)**	**Pt wt%**	**Electrochemical active surface area (m²/g)**	**Onset potential (mV vs RHE)**	**Tafel slope (mV/decade)**	**$j_{0\text{-geometric}}$ (μA/cm²)**	**R_{ct} (Ω)**
Ultralow-Pt-loading bamboo-like nitrogen-doped carbon nanotubes[1]	0.5 M H_2SO_4	-	0.74 wt%	148.5	40	33	-	79
Nitrogen-doped hollow porous carbon polyhedrons embedded with highly dispersed Pt nanoparticles[2]	0.1M $HClO_4$	2.0	-	516	2.7	27	-	-
Ultrathin Pt Layer on Au-Nanoisland- Modified Si Photocathode[3]	0.1 M H_2SO_4	Pt single layer	-	-	120	-	-	-
Single-Walled Carbon Nanotubes with Pseudo-Atomic-Scale Platinum[4]	0.5 M H_2SO_4	0.114 - 0.570	-	-	27	38 - 40	1150 - 1940	-
Ultrafine Pt nanoparticles decorated MoS_2 nanosheets[5]	0.5 M H_2SO_4	66	2.2 wt%	-	31	52	256	8-19
Pt-MoOx/Mo[6]	KOH (PH14)	-		-	24	58	-	-
Pt nanocrystals on nitrogen-doped graphene[7]	-	-	5 wt%	1.69 cm²	24	28	989	1.24
Multiple Carbon Nanotube Yarns and One Platinum Wire[8]	1 M KOH	-	-	-	188	85	-	-
Au(111)-Supported Pt Monolayer[9]	0.1M H_2SO_4	-	-	0.0432 cm²	-	68	630	-
poly(a-terthiophene)-Pt nanoparticle hybrid material (polyTT-Pt)[10]	0.5 M H_2SO_4	8550	2.9 wt%	35.7	67	37	280	570
Pt nanoparticles/MoS_2 nanosheets/carbon fiber[11]	0.5 M H_2SO_4	-	2 wt%	250.2 mF/g	5	53.6	-	-
Pt/C with boron on the surface of support[12]	1M H_2SO_4	-	20 wt%	37	-	-	-	-
Pt40/Vulcan XC-72[13]	1M H_2SO_4	-	40 wt%	40	-	-	-	-

tungsten carbide-supported nano Platinum catalyst[14]	0.5 M H_2SO_4	-	16 wt%	-	-	-	4420	-
Pt nanoparticle on MoS_2 Single layer[15]	0.5 M H_2SO_4	27	36 wt%	-	-	40	-	-
Films of SWCNTs and commercial platinum (Pt) blackweresequentially castonacarbon fiber electrode(CFE)[16]	0.5 M H_2SO_4	1000	-	30.8	-	29	3290	44
Monolayer Platinum on Tungsten Monocarbide Substrates	0.5 M H_2SO_4	-	-	-	-	-	-	-
Pt on Mo_2C[17]	0.1 M $HClO_4$	-	7.2 wt%	-	40	38	6.27	-
Pt/C[18]	-	-	-	-	13	30	1220	-
Pt nanoparticle decorated MoS_2 vertical platelets (this work)	0.5 M H_2SO_4	13	11 wt%	-	9	44	373	-

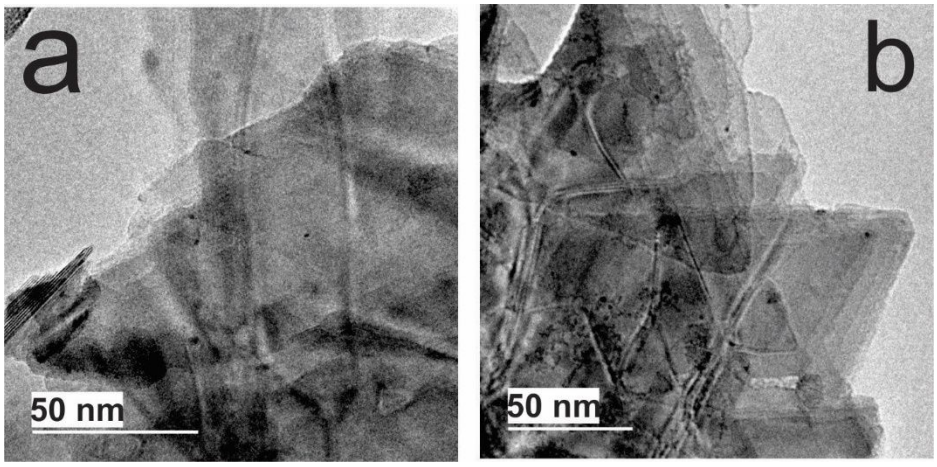

Figure S6. TEM images of the Pt-MoS_2 before and after 10,000 cycling treatment. (0.11 wt% Pt, TA 500 °C)

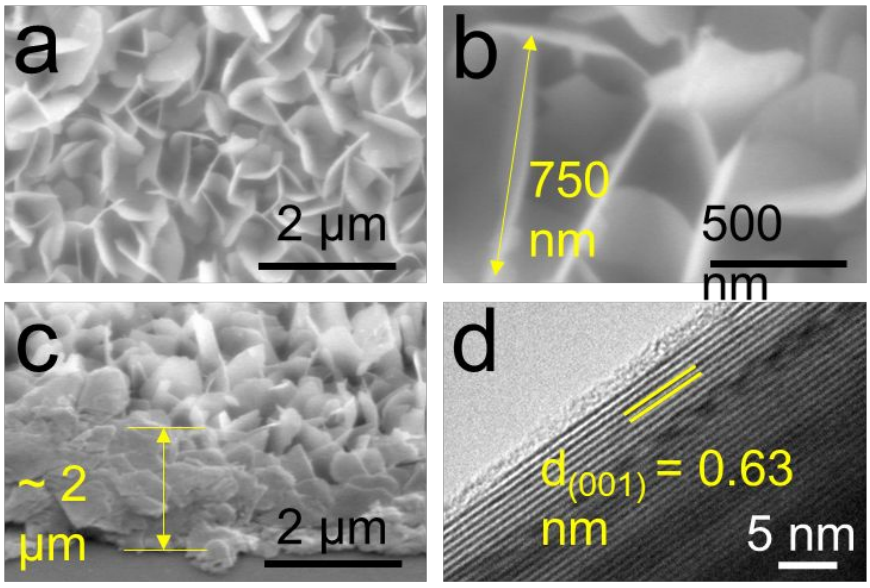

Figure S7. SEM and TEM images revealing the morphology and structure of the CVD MoS_2 thin film. (a,b) Top view SEM images of the MoS_2 thin film. (c) Tilted view SEM image showing the film thickness. (d) TEM image showing the interlayer spacing $d_{(001)}$ of MoS_2 of 0.63 nm.

The SEM and TEM images depicting the structure of the CVD as-grown MoS_2 flakes are shown in Figure S7. SEM images (Figure S7a-c) demonstrate the morphology and thickness of the CVD MoS_2 thin film. As seen in Figure S7a,b, the individual flake size is within the range of 500 – 1000 nm. The film thickness can be measured from tilted SEM image (Figure S7c), to be ~ 2 μm. TEM image in Figure S7d shows the interlayer spacing of 0.63 nm, corresponding to $d_{(001)}$ of MoS_2.

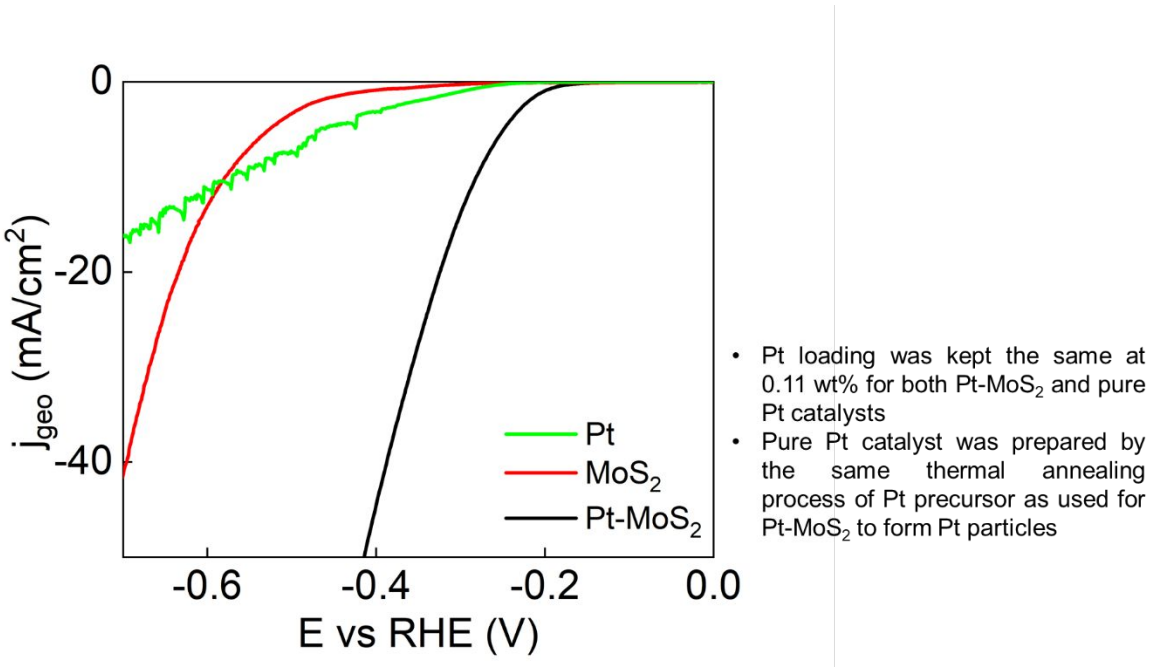

Figure S8. Comparison of HER activity of Pt-MoS_2 with pure MoS_2 and pure Pt catalyst. (Pt loading was kept the same at 0.11 wt%)

Although some of the Pt particles have deposited at the MoS_2 edges, there is still a considerable amount of MoS_2 edges exposing in the resultant Pt-MoS_2 composite as the original MoS_2 edges are only partially covered by Pt crystals. It can be seen in Figure 3, Pt decoration at the MoS_2 edges are discrete that there are edges remaining exposed. Hence, in the catalytic process the remaining MoS_2 edges are believed to participate, which contribute to activity of the composite catalyst. This is in great contract to carbon-based Pt supports that are catalytically inactive and act only as scaffold structurally.

To support this argument, we have performed HER test of the pure MoS_2 and pure Pt (at the same loading 0.11 wt%) catalysts and compared them with the Pt-MoS_2 composite. The results are shown in Figure S8. It's worth noting that the Pt catalysts here was prepared by the same thermal annealing process at the same amount of Pt precursor as used for synthesis of our Pt-MoS_2 composite to facilitate valid comparison and elucidate the role of Pt and MoS_2 in the resultant composite catalyst.

It's found that the composite outperforms its individual counterparts – pure MoS_2 and pure Pt. this result confirms that both Pt and MoS_2 contribute to the catalytic activity of the composite catalyst. Moreover, the fluctuation of HER polarization curve as seen in the pure Pt (green curve) is associated with the constant accumulation and release of the H_2 bubbles. This phenomenon indicates MoS_2 also contributes structurally by providing the superaerophobic surface to maintain a constant working area of the catalyst surface.

Annealing of pure MoS_2.

It's revealed that the annealing process can lead to recrystallization, elimination of defects as well as decrease in degree of vertical alignment of the flakes. Whereas both basal plane defects and edges are active sites of MoS_2 for HER process.[19-22] Therefore, annealing MoS_2 destroys the HER catalytic favourable structures and thus resulted in decreased HER activity.

Some may argue that H_2 annealing could potentially promote the formation of sulphur vacancies (SVs) that can catalyse HER. However, the formation of SVs will only be triggered at high temperature (usually seen 700 °C and above for thin films; 400 °C and above for monolayer).[23-25] Given the thickness of our MoS_2 film and the thermal annealing temperature (400 °C) applied, the formation of SVs is unlikely to occur.

In the event of H_2 annealing of our Pt precursor coated MoS_2, H_2 gas combined with moderate temperature enables reduction of precursor and formation of Pt particles that are highly catalytic active. The activity loss of MoS_2 will be compensated by highly active Pt crystals. Thus, the activity is seen to be greatly enhanced for Pt-MoS_2 when subject to the same annealing process as pure MoS_2.

Supporting References

(1) Park, K. T.; Richards-Babb, M.; Freund, M. S.; Weiss, J.; Klier, K. Surface Structure of Single-Crystal MoS_2 (0002) and Cs/MoS_2 (0002) by X-Ray Photoelectron Diffraction. J. Phys. Chem. 1996, 100, 10739–10745.

(2) Ying, J.; Jiang, G.; Paul Cano, Z.; Han, L.; Yang, X. Y.; Chen, Z. Nitrogen-Doped Hollow Porous Carbon Polyhedrons Embedded with Highly Dispersed Pt Nanoparticles as a Highly Efficient and Stable Hydrogen Evolution Electrocatalyst. Nano Energy 2017, 40, 88–94.

(3) Das, C.; Kot, M.; Rouissi, Z.; Kędzierski, K.; Henkel, K.; Schmeißer, D. Selective Deposition of an Ultrathin Pt Layer on a Au-Nanoisland-Modified Si Photocathode for Hydrogen Generation. ACS Omega 2017, 2, 1360–1366.

(4) Tavakkoli, M.; Holmberg, N.; Kronberg, R.; Jiang, H.; Sainio, J.; Kauppinen, E. I.; Kallio, T.; Laasonen, K. Electrochemical Activation of Single-Walled Carbon Nanotubes with Pseudo-Atomic-Scale Platinum for the Hydrogen Evolution Reaction. ACS Catal. 2017, 7, 3121–3130.

(5) Ren, W.; Zhang, H.; Cheng, C. Ultrafine Pt Nanoparticles Decorated MoS_2 Nanosheets with Significantly Improved Hydrogen Evolution Activity. Electrochim. Acta 2017, 241, 316–322.

(6) Jian, C.; Cai, Q.; Hong, W.; Li, J.; Liu, W. Enhanced Hydrogen Evolution Reaction of MoO_X/Mo Cathode by Loading Small Amount of Pt Nanoparticles in Alkaline Solution. Int. J. Hydrogen Energy 2017, 42, 17030–17037.

(7) Jiang, B.; Liao, F.; Sun, Y.; Cheng, Y.; Shao, M. Pt Nanocrystals on Nitrogen-Doped Graphene for the Hydrogen Evolution Reaction Using Si Nanowires as a Sacrificial Template. Nanoscale 2017, 9, 10138–10144.

(8) Wu, Y.; Wang, Q.; Li, T.; Zhang, D.; Miao, M. Fiber-Shaped Supercapacitor and Electrocatalyst Containing of Multiple Carbon Nanotube Yarns and One Platinum Wire. Electrochim. Acta 2017, 245, 69–78.

(9) Liao, W.; Yau, S. Au(111)-Supported Pt Monolayer as the Most Active Electrocatalyst toward Hydrogen Oxidation and Evolution Reactions in Sulfuric Acid. J. Phys. Chem. C 2017, No. 111, acs.jpcc.7b05259.

(10) Chakrabartty, S.; Gopinath, C. S.; Raj, C. R. Polymer-Based Hybrid Catalyst of Low Pt Content for Electrochemical Hydrogen Evolution. Int. J. Hydrogen Energy 2017, 42, 22821–22829.

(11) Hou, D.; Zhou, W.; Liu, X.; Zhou, K.; Xie, J.; Li, G.; Chen, S. Pt nanoparticles/MoS_2 Nanosheets/carbon Fibers as Efficient Catalyst for the Hydrogen Evolution Reaction. Electrochim. Acta 2015, 166, 26–31.

(12) Ma, H. C.; Xue, X. Z.; Liao, J. H.; Liu, C. P.; Xing, W. Effect of Borohydride as Reducing Agent on the Structures and Electrochemical Properties of Pt/C Catalyst. Appl. Surf. Sci. 2006, 252, 8593–8597.

(13) Grigoriev, S. A.; Millet, P.; Fateev, V. N. Evaluation of Carbon-Supported Pt and Pd Nanoparticles for the Hydrogen Evolution Reaction in PEM Water Electrolysers. J. Power Sources 2008, 177, 281–285.

(14) Sheng, J. F.; Ma, C. A.; Zhang, C.; Li, G. H. Preparation of Tungsten Carbide-Supported Nano Platinum Catalyst and Its Electrocatalytic Activity for Hydrogen Evolution. Wuli Huaxue Xuebao/ Acta Phys. - Chim. Sin. 2007, 23, 181–186.

(15) Huang, X.; Zeng, Z.; Bao, S.; Wang, M.; Qi, X.; Fan, Z.; Zhang, H. Solution-Phase Epitaxial Growth of Noble Metal Nanostructures on Dispersible Single-Layer Molybdenum Disulfide Nanosheets. Mol. Ther. 2013, 4, 1444.

(16) Girishkumar, G.; Rettker, M.; Underhile, R.; Binz, D.; Vinodgopal, K.; McGinn, P.; Kamat, P. Single-Wall Carbon Nanotube-Based Proton Exchange Membrane Assembly for Hydrogen Fuel Cells. Langmuir 2005, 21, 8487–8494.

(17) Regmi, Y. N.; Waetzig, G. R.; Duffee, K. D.; Schmuecker, S. M.; Thode, J. M.; Leonard, B. M. Carbides of Group IVA, VA and VIA Transition Metals as Alternative HER and ORR Catalysts and Support Materials. J. Mater. Chem. A 2015, 3, 10085–10091.

(18) Jahan, M.; Liu, Z.; Loh, K. P. A Graphene Oxide and Copper-Centered Metal Organic Framework Composite as a Tri-Functional Catalyst for HER, OER, and ORR. Adv. Funct. Mater. 2013, 23, 5363–5372.

(19) Guo, B.; Yu, K.; Li, H.; Song, H.; Zhang, Y.; Lei, X.; Fu, H.; Tan, Y.; Zhu, Z. Hollow Structured Micro/Nano MoS_2 Spheres for High Electrocatalytic Activity Hydrogen Evolution Reaction. ACS Appl. Mater. Interfaces 2016, 8, 5517–5525.

(20) Gaur, A. P. S.; Sahoo, S.; Ahmadi, M.; Guinel, M. J. F.; Gupta, S. K.; Pandey, R.; Dey, S. K.; Katiyar, R. S. Optical and Vibrational Studies of Partially Edge-Terminated Vertically Aligned Nanocrystalline MoS_2 Thin Films. J. Phys. Chem. C 2013, 117, 26262–26268.

(21) Kong, D.; Wang, H.; Cha, J. J.; Pasta, M.; Koski, K. J.; Yao, J.; Cui, Y. Synthesis of MoS_2 and $MoSe_2$ Films with Vertically Aligned Layers. Nano Lett. 2013, 13, 1341–1347.

(22) O'Neill, A.; Khan, U.; Coleman, J. N. Preparation of High Concentration Dispersions of Exfoliated MoS_2 with Increased Flake Size. Chem. Mater. 2012, 24, 2414–2421.

(23) He, M.; Kong, F.; Yin, G.; Lv, Z.; Sun, X.; Shi, H.; Gao, B. Enhanced Hydrogen Evolution Reaction Activity of Hydrogen-Annealed Vertical MoS_2 nanosheets. RSC Adv. 2018, 8, 14369–14376.

(24) Ye, G.; Gong, Y.; Lin, J.; Li, B.; He, Y.; Pantelides, S. T.; Zhou, W.; Vajtai, R.; Ajayan, P. M. Defects Engineered Monolayer MoS_2 for Improved Hydrogen Evolution Reaction. Nano Lett. 2016, 16, 1097–1103.

(25) Lin, Z.; Mccreary, A.; Wurstbauer, U.; Miller, B.; Ponraj, J. S.; Xu, Z.; Lin, Z.; Carvalho, B. R.; Kahn, E.; Lv, R.; et al. Defect Engineering of Two-Dimensional Transition Metal Dichalcogenides Defect Engineering of Two-Dimensional Transition Metal Dichalcogenides. 2016, 3, 022002.